TECHNICAL PAPER

Fast response and recovery of nano-porous silicon based gas sensor

V. S. Selvakumar[1] · L. Sujatha[2]

Abstract

Fusion of the transduction mechanism in micro and macro nanopores of porous silicon (PS) was employed to fabricate an MEMS-based aliphatic alcohol impedance sensor. The presence of a nanopore network on silicon was confirmed by the SEM image. The morphology of the PS nanopores was roughly distributed in a uniform manner. The performance of the sensor was studied using Impedance spectroscopy at room temperature. Electrochemical impedance spectroscopy and an equivalent circuit analysis of the small amplitude ($\pm$ 10 mV) AC impedance measurements (frequency range 0.1 Hz–1 kHz) at ambient temperature were carried out. The Sensing layer consists of nanopores (45.30–71.13 nm), micropores (0.95–5 μm), and comb type alumina electrodes with the micro PS layer having a thickness of about 0.2 μm and the macro PS layer having a thickness of about 4 μm. These results were used to assess the effect of the micro PS and macro PS of the particulate layer on the conductivity of the given aliphatic gases. The measured impedance was approximately 2.3e5 for the micro PS, and 3.22e5 macro PS for 8 ppm of gas injected into the gas chamber. The grain boundary resistance increases with an increase in the concentration of butane, benzene, and methane, which ranges from 2 to 16 ppm.

1 Introduction

The primary need of the day is to constantly monitor air quality levels in laboratories, hospitals, generic technical installations and to control air pollution in the environment. A highly effective gas sensor is needed in order to monitor it. The same is also used in machines such as breath analyzers and also to monitor fermentation and other such chemical processes. All these requirements necessitate the fabrication of highly sensitive gas sensors to avoid accidents caused by gas leakages. Such a sensor should allow continuous monitoring of the concentration of the target gases in the environment. An ideal gas sensor should have advantageous characteristics, such as high sensitivity, high selectivity, rapid recovery, small size, low cost, and repeatability (Pérez 2008). Micro PS is the oldest PS material, which is generally formed by using aqueous electrolytes with high HF concentrations on p-type silicon of moderate resistivity and the Micro PS layers grow

rapidly. The porous silicon offers a very high ratio of surface area/volume which increases the volume of gas interaction, i.e. which increases the reaction rate of gas detection (Wang et al. 2008). They have a wide range of structures (from macroporous with a pore diameter of over 50 nm to microporous with a pore diameter of under 2 nm) having a very large surface to volume ratio, ease of fabrication, distributed nature of resistive capacitance network, natural nanocrystalline quantum wire like behaviour and compatibility to silicon IC technology leading to smart sensors. These features have fascinated researchers throughout the world for more than a decade (Badilla et al. 2011; Valera et al. 2007; du Plessis 2007).

PS is also an effective platform for the sensing of methane, benzene and butane. In fact, the high volume to area ratio of PS makes the substrate an ideal choice for gas detection. A wide range of manufacturing techniques have been developed for the construction of gas sensitive porous silicon (Sailor 2012; Losic and Santos 2015). In each case, the sensing parameters of PS were highly dependent upon the manufacturing process. Critical steps within the manufacturing process include the proper preparation of the etching solution, the electrical potential of the etch and the etching time. Additionally, factors such as the silicon's orientation and the geometry of the etching cell are critical in the formation of the porous silicon (Palzer et al. 2008; Zhang 2005). The collective effect of these parameters

✉ V. S. Selvakumar
selvakumar.vs@rajalakshmi.edu.in

1 Department of Electronics and Communication, Rajalakshmi Engineering College, Chennai, India

2 Centre of Excellence in MEMS and Microfluidics, Rajalakshmi Engineering College, Chennai, India

enables many different PS formations. The most applicable example of PS formation for chemical sensing is the two contact rapidly reversible PS gas sensor (Ogata et al. 2007; Escorcia-Garcia et al. 2009).

In general, the gas detection is done by measuring the variation of electrical and other such properties with changes in gas concentration. PS based gas sensing by the gas injection method and signal processing will be described, and the attributes of the existing technologies that are significant to PS and its characterization will be detailed. (Zhang et al. 2014; Sujatha and Bhattacharya 2007a).

Usually, PS based gas sensors are used to monitor benzene, butane, and methane at room temperature at the ppm level. The complete mechanism involving changes in grain resistance and grain boundary contribution during the interaction of the nanopores with the target gases has been proposed. AC impedance spectroscopy has been used in the present study to determine the sensitivity of the sensor, though only DC methods are used to detect toxic gases (Gessner et al. 2000; Kanungo and Basu 2014).

Porous silicon semiconductor (PS) gas sensors offer a technology platform for rapid, low cost, portable gas measurement. When defining the operating characteristics of porous silicon, it is critical to benchmark the device performance against the current state of the art. The most common method of electrical contact taken from the PS layer is two contact probing which is investigated in this report. This attribute is achieved through low resistance ohmic contacts that are formed on the device's surface. (Vinod 2005; Kanungo et al. 2009; Sujatha and Bhattacharya 2007b; Mabrook et al. 1995).

Based on the literature, our proposed research work focuses on the fabrication of a PS based gas sensor with characteristics, such as good sensitivity, selectivity, and repeatability at room temperature. Thus, for all practical purposes, room temperature is the ideal temperature along with superior stability, sensitivity and rapid response time of a sensor. The primary goal of this research is to bring up a competitive impedance metric analysis for two-point metal contact and series/parallel contacts on PS layer based gas sensor applications (Selvakumar and Sujatha 2019; Kanungo et al. 2006; Dusheiko et al. 2017; Selvakumar et al. 2019; Karacali et al. 2013).

2 Materials and methods

The sensor chip is made of a sensitive film and interdigitated electrodes. There are various steps involved in the fabrication of the alcohol sensor that are explained in detail below.

2.1 Wafer cleaning

The removal of chemical and particle impurities such as metals, particles, contaminants, native oxides, and micro roughness without altering or damaging the wafer surface or substrate, is the main objective of the wafer cleansing process. A P-type Silicon wafer of thickness 525 μm, with 100 orientation, polished on one side, having a resistivity of 1–10 Ωcm and a diameter of 4 inches is used. Standard cleaning procedure is used to clean the wafer. A Diamond cutting tool is then used to cut the wafer into samples of size 2 cm × 2 cm. The results of the *wafer cleaning process such as roughness, corrosion or pitting can be negated by maintaining the surface of the wafer properly.*

2.2 Thermal evaporation

Evaporation is a common method used for thin-film deposition. The source material (aluminum) is evaporated in a vacuum. The vacuum allows vapor particles to travel directly to the target object (P-type silicon), where they condense back to a solid state.

2.3 Electrochemical wet etching porous silicon

P-type Silicon wafer of thickness 525 μm, with 100 orientation, polished on one side, having a resistivity of 1–10 Ωcm and a diameter of 4 inches is used. The Wafer is cleaned by standard cleaning procedure. It is then cut into samples of size 2 cm × 2 cm using a diamond cutting tool. Figure 1 shows the schematic of the formation of PS by electrochemical wet etching in a hydrofluoric acid (HF) based electrolyte. The experimental setup of a novel constant current source is constructed for the formation of porous silicon. To obtain a uniform morphology of porous silicon by electrochemical etching requires a constant current source; we have designed a constant current source by using an operational amplifier, a zener diode and some passive components. It provides a constant current (1–50 mA) to the wet electrochemical etching for forming a uniform geometry and morphology. In order to provide a uniform current distribution across the surface, an aluminium layer was deposited on the back side of the silicon samples. The Silicon sample was placed at the bottom of a cylindrical cell made of Teflon and fixed using a stainless steel plate as a backing material. The silicon sample acts as the anode and a platinum rod acts as the cathode.

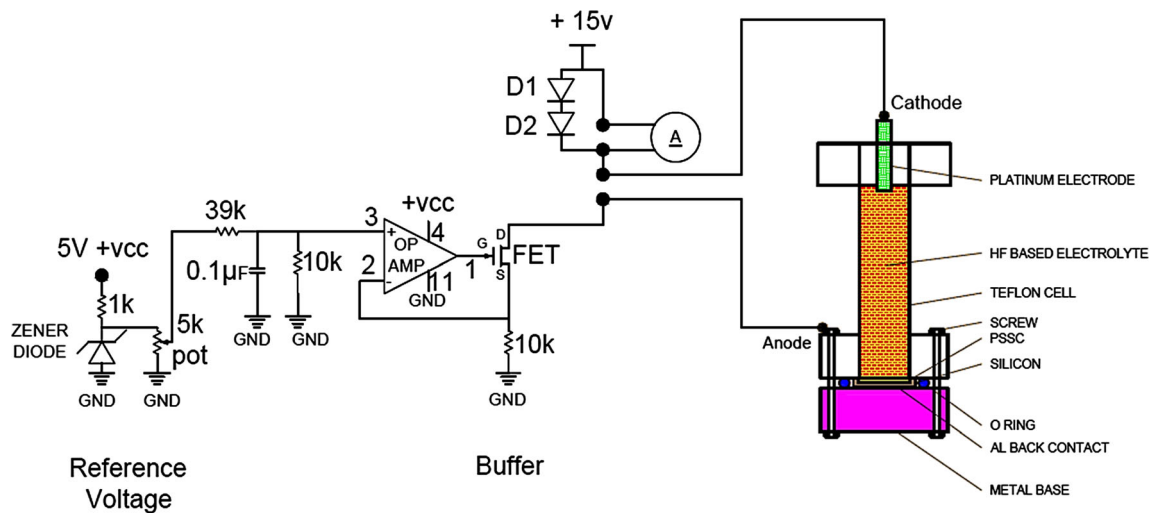They were separated by a distance of 9 cm. The etching was carried out by varying the time duration of the etching

Fig. 1 Experimental setup for wet electrochemical etching of silicon in our laboratory

process with a concentration of 48–50% HF. The electrolyte for the micro PS is the combination of hydrofluoric (HF) and isopropyl alcohol (IPA). The electrolyte for the macro PS is the combination of HF and dimethyl formamide (DMF).

A constant current was supplied between the two electrodes immersed in Teflon cell containing an aqueous solution of HF and IPA. Thus, the IPA or DMF reduced the hydrogen bubble throughout the process. The electric current was supplied using an ADCMT 6243 and DC current source. A constant current is applied through the circuit and the PS samples were prepared for various timings and HF concentrations. Similarly, the PS was formed for various current densities also.

2.4 IDE contacts on PS based alcohol gas sensor

The interdigitated electrodes (IDEs) are composed of two interdigitated electrodes with two connection tracks, on a PS substrate. These IDEs offer several advantages, such as working with low volumes of samples and avoiding tedious polishing of solid electrodes. The interdigitated configuration typically enhances the sensitivity and detection limits. It consists of 2D and 3D cross sectional views of the alcohol sensor. It is obtained by the IDEs by aluminum thermal evaporation with shadow mask techniques. The thickness of the IDEs is 0.1 μm.

Figure 2 shows the fabricated and 3D diagrammatical view of the IDE's structure on the porous silicon. Figure 3 shows the schematic and systematic procedure for the fabrication of the PS-based gas sensor.

3 Alcohol gas testing schematic and experimental setup

The performance of the developed PS based gas sensor for measuring various gases was evaluated. Gas sensitivity is measured using the static gas system which is schematically represented in Fig. 4a. The experimental setup used for recording the performance of the alcohol gas sensor using an electrochemical workstation is presented in Fig. 4b. From the pre-calibrated gas canister, a known amount of gas was taken out using an airtight syringe and then injected into a known volume of the testing chamber provided with rubber septum as an injection port.

A known concentration of the benzene, butane and methane gas was passed into the chamber with the help of an airtight syringe. The AC impedance technique was used to evaluate the sensor's interaction with the above-mentioned gases. A frequency range of 0.1 Hz–1 kHz was generated using a small AC signal of 10 mV. The response was obtained using a frequency response analyser attached with a Potentiostat (BioLogic; SP240). Impedance spectroscopy was recorded for benzene, butane and methane at room temperature in ambient air conditions.

4 Characterisation part

4.1 Optical microscope

The magnification of a simple optical microscope is about ten times (10 ×).To increase the magnification we used a compound microscope that consists of two types of lenses that enhance the magnification to about 15 times (15 ×).

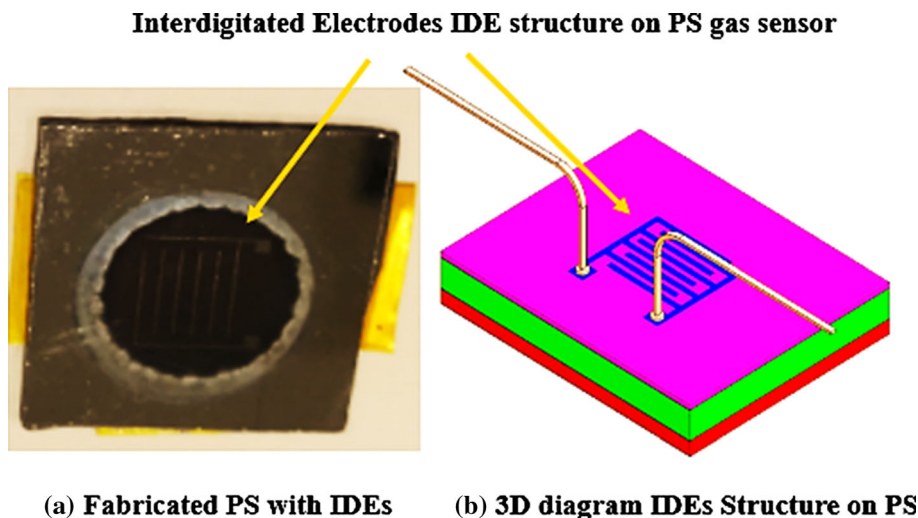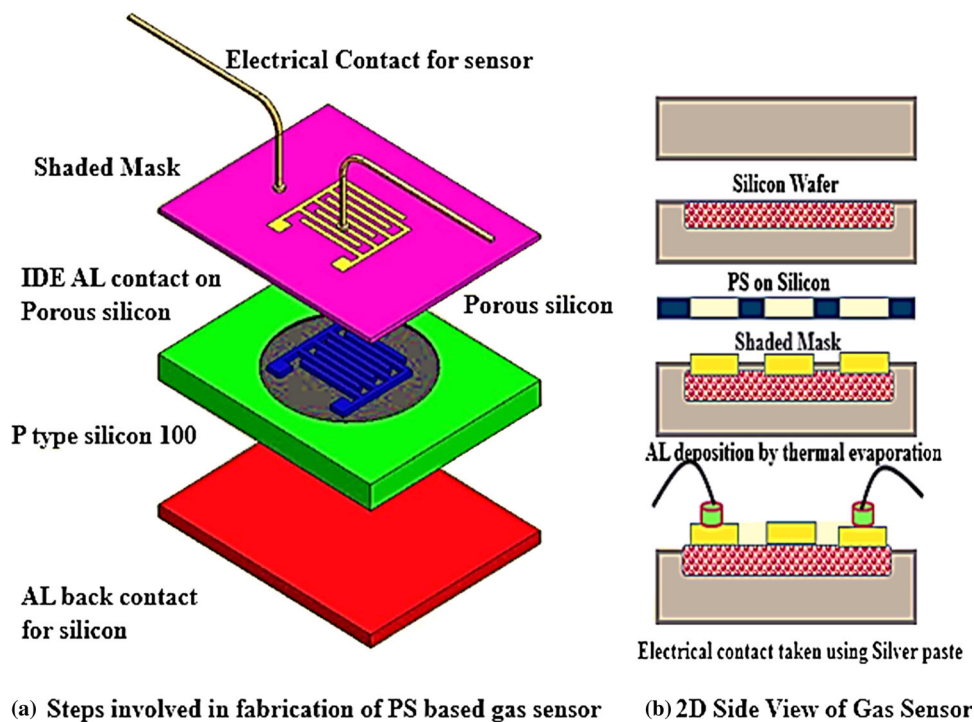**Fig. 2** IDE's structure on porous silicon based gas sensor

Interdigitated Electrodes IDE structure on PS gas sensor

(a) Fabricated PS with IDEs (b) 3D diagram IDEs Structure on PS

Fig. 3 Top view and side view of porous silicon based alcohol gas sensor

(a) Steps involved in fabrication of PS based gas sensor (b) 2D Side View of Gas Sensor

4.2 MiniSEM

The Surface morphology of the micro and macro PS is characterised by using a MiniSEM (SNE 4500 m) scanning electron microscope. The specification of the MiniSEM is as follows: magnification up to 60,000 × (digital zoom 4 ×) detector: SE detector BSE detector—multi mode variable accelerating voltage from 5 to 30 kV (5 steps) sample loading time < 2 min. Auto focus, Auto brightness and contrast max. Sample size: 60 mm in diameter, 25 mm in height laptop or desktop control with Microsoft Windows7 OS Dimension: 390 mm (W) × 640 mm (D) × 560 mm (H).

4.3 Profilometer

ContourGT-X8 PSS Optical Profiler is Based on Bruker's flagship Contour GT;, the ContourGT-X8 PSS provides highly-repeatable, high throughput, precision surface metrology of high-brightness LED (HB-LED) patterned sapphire substrates (PSS) for the production of QA/QC environments. Offering seamless integration with
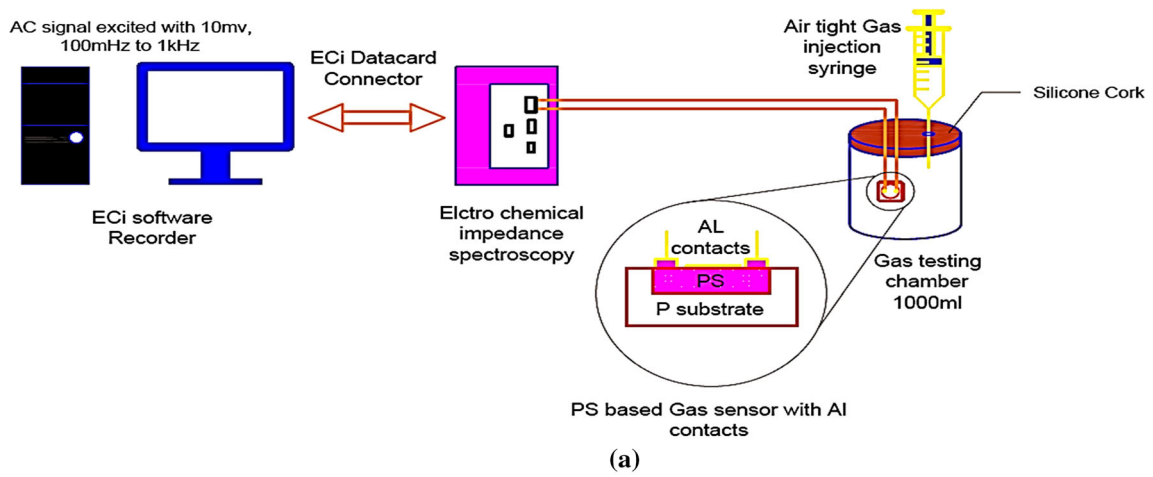
(a)

(b)

Fig. 4 **a** Schematic representation of benzene, butane and methane gas sensing experimental setup. **b** Experimental setup used for recording the performance of benzene, butane and methane gas sensor using electrochemical workstation

Table 1 Specification of 3D non-contact (contour GT)

Specifications	
Measurement throughput	≤ 5 s per measurement
PSS measurement field of view (FOV)	$\sim 20\ \mu m^2$
PSS features measured per FOV	Typically 20–100, with simultaneous measurements of height, width and pitch
Approximate throughput	≤ 2 min per 2-inch wafer with 13 sites (depending on wafer handler throughput)
3σ repeatability (20 measurements)	Height: ≤ 6 nm; width: ≤ 15 nm; pitch: ≤ 4 nm
Long term stability (5 days)	≤ 8 nm, 3σ height repeatability

automated substrate handlers, the ContourGT-X8 PSS enables manufacturers to obtain nanometer-level accuracy and repeatability while simultaneously measuring the height, width and pitch of multiple PSS features with 230 × magnification (Table 1).

5 Results and discussion

P-type Silicon < 100 > orientation, 525 μm thick, Single side polished, 10 Ω-cm wafers are used to form the PS. The variation in porosity and thickness depends on the chemical dissolution during PS formation. Increase in current density increases the rate of PS formation and hence, the porosity increases (Table 2).

The porosity (P) and thickness (d) of the PS are calculated by means of the gravimetric method using Eqs. (1) and (2) respectively. The samples are weighed before anodization (m_1), just after anodization (m_2), and after dissolution of the porous silicon layer in 3% KOH solution (m_3).

$$P(\%) = \frac{m_1 - m_2}{m_1 - m_3} \times 100 \tag{1}$$

$$d = (m_1 - m_3)/\rho S \tag{2}$$

where ρ is the Si density and S is the anodized surface area.

Table 2 shows the increase in porosity with the increase in current density for both Micro PS and Macro PS for HF concentrations of 33%, 50% and 66% for the anodisation time of 10 min.

5.1 Study of porous silicon morphology

The microscopic image of the PS was obtained using a scanning electron microscope (SEM). It produces images of a sample by scanning it using a focused beam of electrons.

From Fig. 5a, b we can see the clear difference between the Micro PS and Macro PS. Figure 5a, b shows the SEM images and profiler images of the Micro PS and Macro PS respectively with 50% porosity.

It is observed that the pore sizes are in the range of 45.30–71.13 nm in the micro PS and in the range of 0.95–5 μm in the macro PS. In addition, the pores in the micro PS are random in nature, whereas the pores in macro PS are very uniform. Profiler is a 3D interactive display of the displacement sensor that creates a profile of the surface by collecting the height data and it is used to measure the height, width, angle, radius, position, and more.

Figure 6 and 7 shows the profiler images of the micro and macro PS. Both the SEM and profiler images show that the micro PS is random in nature whereas the macro PS is uniform.

Figure 8a, b show the photographs of the visible photo luminescence of the micro and macro PS with 50% HF concentration, 10 mA/cm^2 current density and 10 min of anodisation time. The PL intensity is higher in the micro PS compared to the macro PS due to the nanometer size pores and hence, the PL is very bright orange for the micro PS and dull orange for the macro PS, as shown in the figure the visible photoluminescence (PL) emission on both the micro and macro PS is under a UV light of 365 nm in a chamber. It is observed that there is a yellow colour PL on the micro PS and an orange colour PL on the macro PS.

5.2 Impedance metric method

Generally, these sensors contain porous silicon consisting of nanopores. Reference to external air is not necessary however; the sensor must be calibrated in order to correlate the signal to known gas concentrations. First, the gases diffuse to the electrode surfaces, where they adsorb, dissociate, and diffuse along the surface to the electrode–porous silicon interface, followed by charge transfer reactions. Then, an ion transport through the PS occurs with

Table 2 Formation parameters of the micro and macro PS

Formation parameter	Porosity 65%		Porosity 70%		Porosity 75%	
	Micro PS	Macro PS	Micro PS	Macro PS	Micro PS	Macro PS
Time (min)	6.5	6	8	10	10	12
Current density (mA/cm^2)	5	5	7	10	8	10
HF concentration (%)	66	33	66	33	50	50

Fig. 5 Microscopic images of **a** micro PS and **b** macro PS

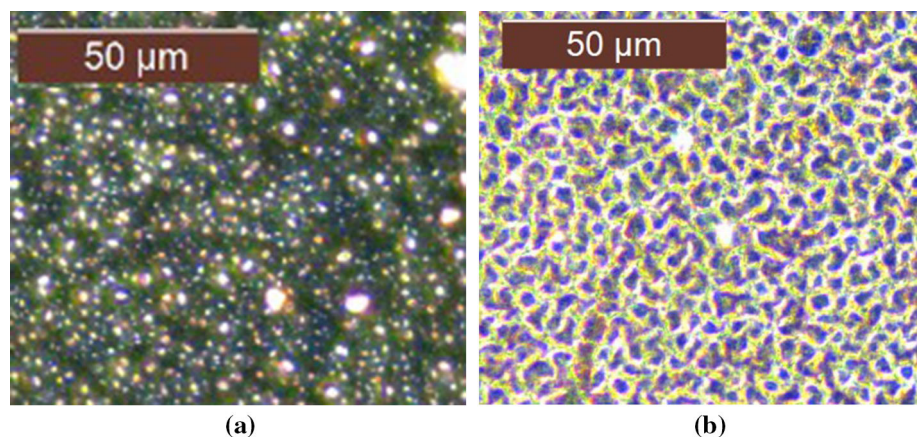(a)   (b)

Fig. 6 SEM picture of **a** micro PS, **b** macro PS
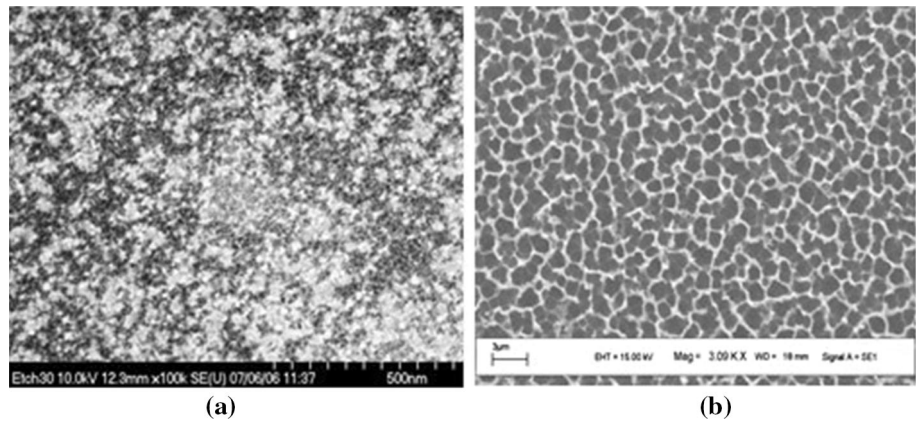

(a)   (b)

Fig. 7 PS formed on **a** aqueous electrolyte and **b** organic electrolyte

(a)   (b)
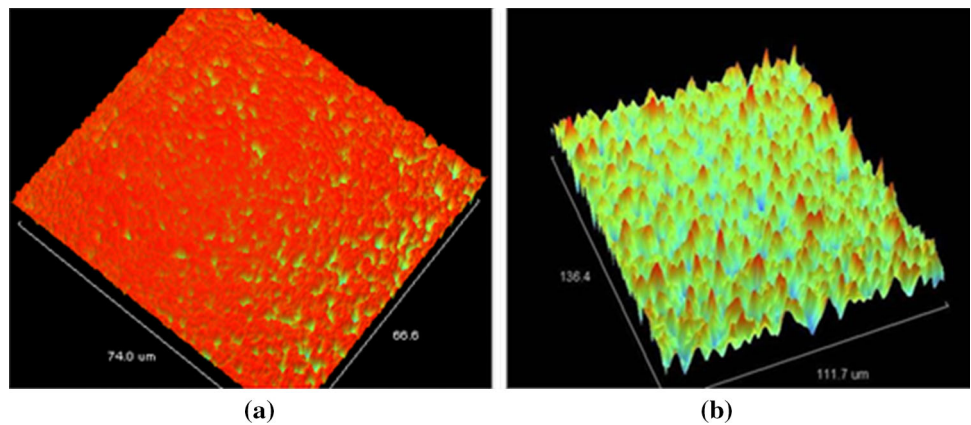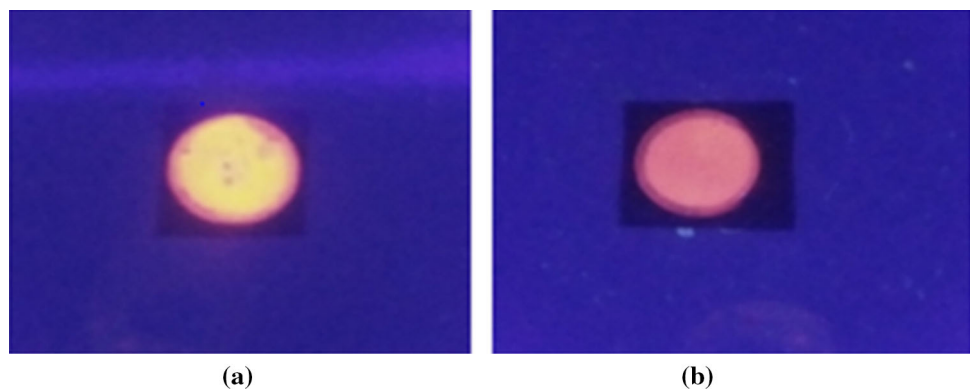
Fig. 8 PL emission from porous silicon **a** micro PS, **b** macro PS

(a)   (b)

charge transfer across the grain boundaries. At various frequencies, some of the processes may contribute to the impedance response, depending on the surface geometry and morphology when reacting with aliphatic alcohols.

The response of the developed layer of PS was analysed for its benzene, butane, and methane sensing ability by impedance spectroscopy. A remarkable change in the impedance parameters was observed in the Nyquist plot. The sensing property of this device is contributed by the unique morphological nature of the PS layers and its changes in the impedance measurements. Figure 9 shows that the changes

in resistance are contributed by three areas—grain bulk ($R_1 R_2$), grain boundaries ($Q_1 R_2$) and the Aluminium on the PS contact ($R_2 Q_2$). The Nyquist plots obtained during exposure of the PS to benzene concentrations ranging from 2 to 8 ppm are shown in Fig. 9 as two incomplete semicircles. The fitted curves are shown by solid lines and the measured values are marked as solid symbols. The diameter of the semicircle was found to increase with the increase in concentration of aliphatic alcohol. The resistance and capacitance values are obtained from the curves. The total impedance of the proposed equivalent circuit is given by,
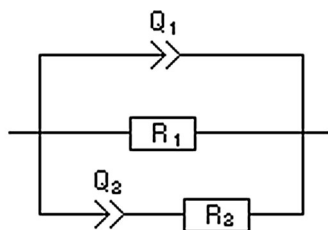
Impedance

$$Z(f) = \frac{R_1 R_2}{R_2 + R_1 (1 + (j2\pi f)^{\alpha_1} Q_1 R_2 + (j2\pi f)^{\alpha_2} Q_2 R_2)}$$
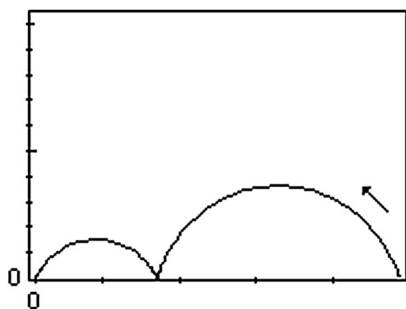
Nyquist Diagram (-Im[Z] vs. Re[Z])

Fig. 9 Equivalent circuit of PS sensor for detection gases

$$z(f) = \frac{R1R2}{R2 + R1(1 + (J2\Pi F)Q1R2 + (J2\Pi F)Q2R3)} \qquad (3)$$

where Q1—constant phase element (CPE) of the PS bulk, R1—resistance of the PS bulk, Q2—CPE of the electrode/PS/gas interface, R2—resistance of the electrode/PS/gas interface, a1, a2—component associated with CPE

Gas concentration calculation using a precalibrated gas cylinder

$$A = \frac{Chamber\ volume\ in\ ml}{Gas\ taken\ in\ air\ tight\ syringe} \qquad (4)$$

$$B = \frac{Gas\ concentration\ in\ a\ cylinder}{A} \qquad (5)$$

modulus of Z_a = Impedance in air, modulus of Z_{g} = Impedance in gas

5.3 Selectivity (S)

$$S = \frac{Za}{Zg} \qquad (6)$$

5.4 Sensitivity

The rate-limiting processes that occur at particular frequencies appear in the impedance spectra. Figure 8 shows

a typical Nyquist plot of data recorded from a PS based sensor with an Al working electrode at room temperature. The plot shows the results of two measurements made when the sensor was exposed to three different gases: (1) benzene (2) methane and (3) butane. A Nyquist plot shows the resistive and capacitive contributions of impedance, but it does not explicitly show the frequencies, so the six decades of frequency are indicated. The low frequency arc (approximately f < 104 Hz) varies in the presence of various gas species; it is sensitive to transport events. The effect of aliphatic gases is to shift the low frequency arc outwards. Both the modulus, |Z|, and the phase angle, |O|, change as a result. The modulus represents the length of the vector from the origin to an impedance measurement at a specific frequency (10 Hz). The phase angle is the arctangent of the ratio of the capacitive contribution of the impedance to the resistive component at a specific frequency. Upon exposure to an analyte gas, the changes in the modulus and phase angle are linear over a specific range of gas concentration at a given frequency. An aliphatic gas sensor needs only to interrogate one frequency typically in the low frequency range (typically f < 1000 Hz). The frequency is selected as a compromise between the speed of response, which favours higher frequencies, and sensitivity, which favours lower frequencies.

Figure 9 shows the Impedance variation of the Micro PS and Macro PS. Electrochemical impedance spectroscopy (EIS) and an equivalent circuit analysis of the small amplitude ($\pm$ 5 mV) AC impedance measurements (frequency range 1 kHz–0.1 Hz) at ambient temperature were carried out. It clearly indicates that the imaginary part of impedance increases with an increase in the benzene, butane and methane gas concentration from 2 to 16 ppm. It was observed that the calculated average impedances were approximately around 2.3e5 for the micro PS, and 3.22e5 for the macro PS of 8 ppm injected gas into the gas chamber respectively. From Fig. 9, it is observed that the Micro PS has higher level changes with respect to the gas injection.

From Fig. 10, is observed the rate of change of Imaginary impedance with respect to benzene, methane gas injection to the testing chamber. The effect of benzene gas injection is to shift the low frequency arc outwards. Both the modulus, |Z|, and phase angle, |O|, change as a result.

From Figs. 11, 12 and 13, it is observed that the calculated impedances were approximately around 5.9e5 for benzene gas, 4.03e5 for Methane gas and 4.9e5 for butane gas of 6 ppm with respect to the air in the testing gas chamber respectively.

The optimized PS morphology to sense the low ppm level (from 2 to 8 ppm and 16 ppm) and also maximum change in impedance have been noted in this range of gas
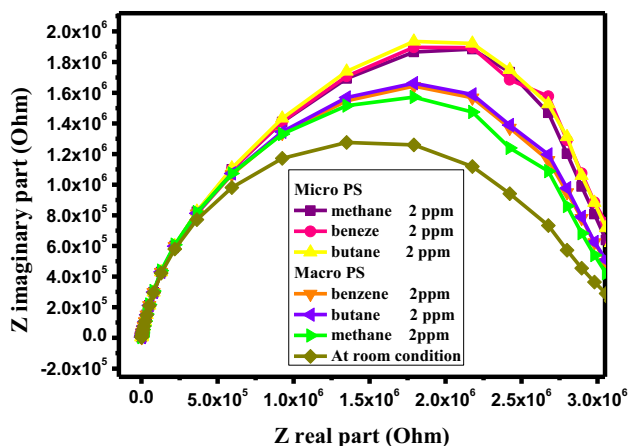
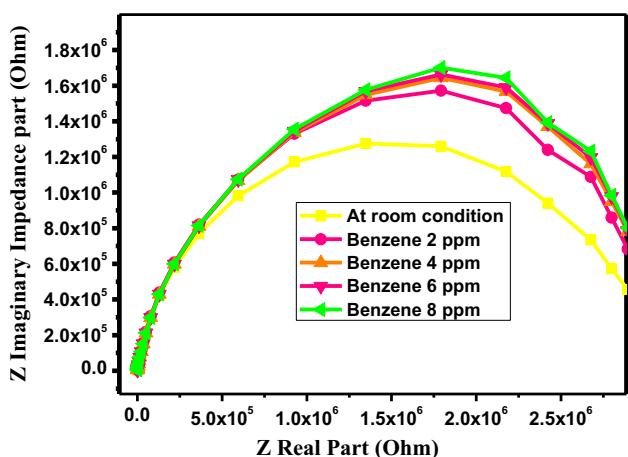Fig. 10 Sensitivity comparison of micro and macro PS

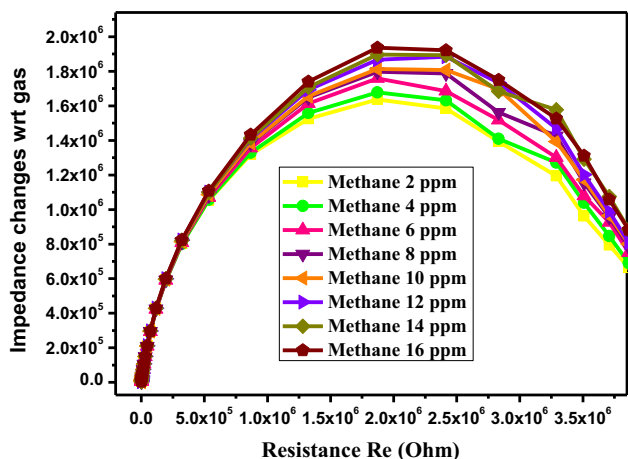Fig. 11 Micro PS based gas sensor measurement of resistance changes for benzene

Fig. 12 Micro PS based gas sensor measurement of resistance changes for methane

concentration. The sensor is saturated if the concentration goes beyond 16 ppm. The focus range of the developed
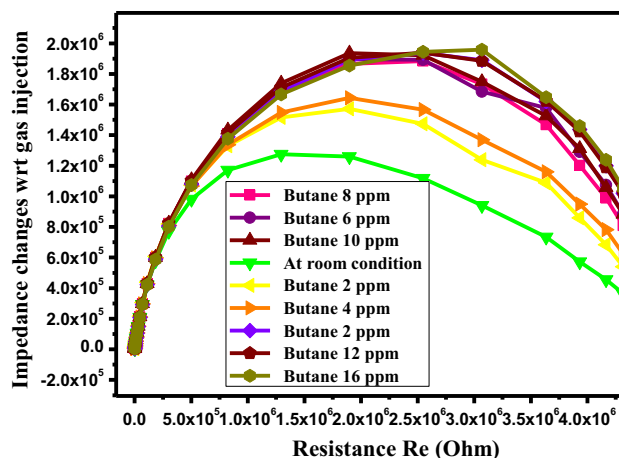

Fig. 13 Micro PS based gas sensor measurement of resistance changes for butane

sensor is 2–16 ppm. It can be observed in the above Figs. 10, 11, 12 and 13.

The percentage value of the sensor selectivity towards benzene, butane, methane along with other interfering gases was measured using the formula given in Eqs. (4) and (5). Figure 16 shows the selectivity of the PS towards aliphatic alcohol with respect to various gases at 100 Hz. The sensitivity percentage of the sensor towards benzene is found to be more when compared to other gases.

5.5 Repeatability

It is understood that repeatability is the range of acceptable values the sensor will read, relevant to a previous measurement, when measuring a gas, independent of the actual gas concentration. Figure 15 shows clearly that the sensing action remains unchanged for repeated measurements.

The percentage value of the sensor selectivity towards benzene, butane, methane along with other interfering gases was measured using the formula given in Eq. (4). Figure 16 shows the selectivity of the PS towards aliphatic alcohol with respect to various gases at 100 Hz. The sensitivity percentage of the sensor was found to be more when compared to other gases.

5.6 Response, recovery and repeatability

It was observed from Fig. 17 that the response and recovery of the sensor are about 12 s and 8 s respectively. This indicates the response and recovery performance of the developed sensor towards benzene, butane and methane gas. The calculated imaginary impedance was approximately $8.2e^5$ for benzene, 3.1e5 for methane and for butane
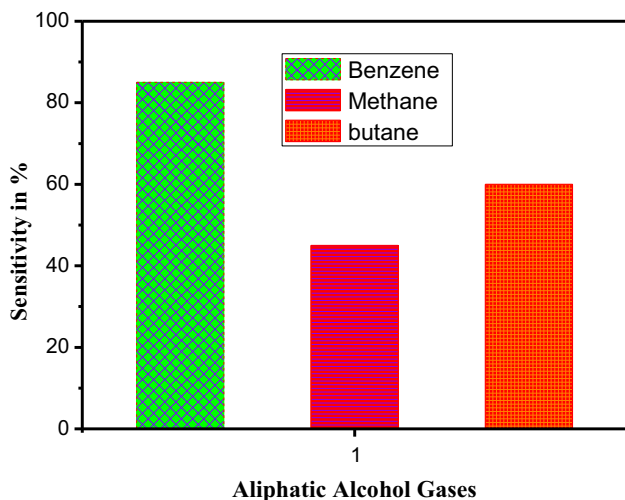
Fig. 14 Sensitivity chart of various alcohol gases to 8 ppm at 100 Hz at room temperature
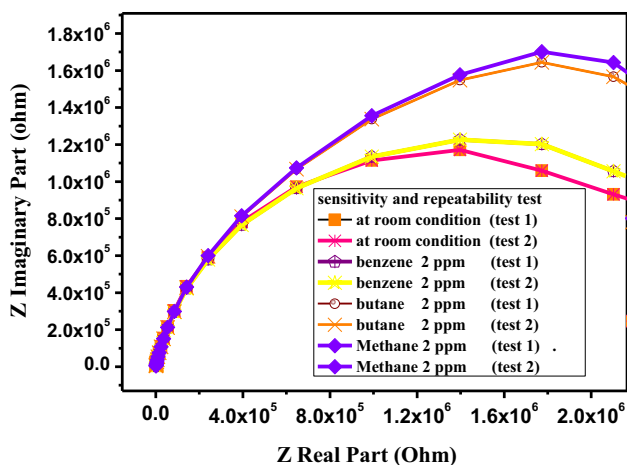

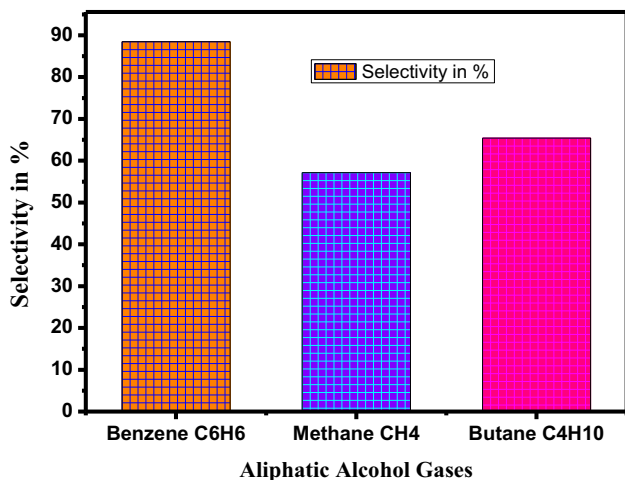Fig. 15 Sensor repeatability of the PS based gas sensor

Fig. 16 Selectivity chart of alcohol gases for 8 ppm of various gases at 10 Hz at room temperature

$4e^5$ for 6 ppm of gas injected into the gas chamber. The grain boundary resistance increases with an increase in the concentration of butane, benzene, and methane, which ranges from 2 to 8 ppm.

It was observed that the response and recovery of the sensor are about 2 s and 6 s respectively. This indicates the response and recovery performance of the developed sensor towards benzene, butane and methane gas. Figure 18 shows the various quick responses and recoveries of benzene, butane, methane gases that clearly prove the selectivity of these gases by measuring different impedances. The PS sensor is very sensitive to benzene gas when compared to all other gases (Figs. 14, 15, 16).

Figure 17 shows the various quick responses and recoveries of benzene, butane, methane gases that clearly prove the selectivity of these gases by measuring different impedances. The PS sensor is very sensitive to benzene gas when compared to all other gases.
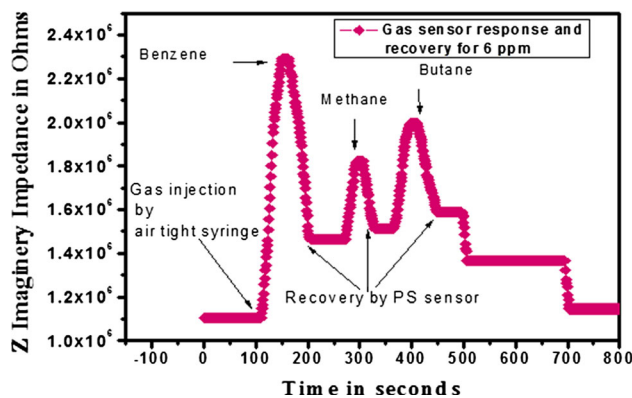

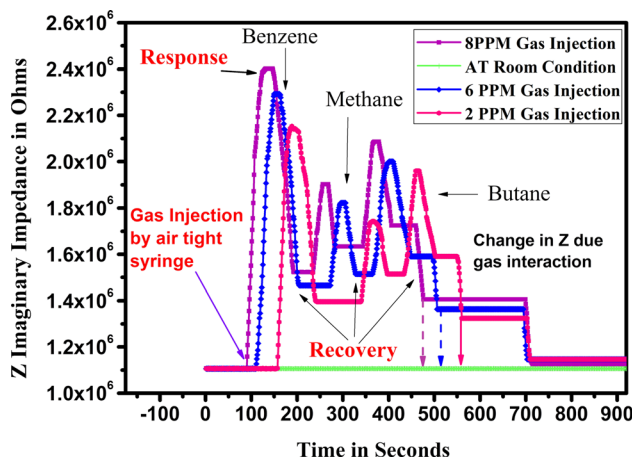Fig. 17 MEMS based gas sensor response, and recovery

Fig. 18 Gas sensor response of various gases with different concentrations

5.7 Z fit for the PS sensor and its equivalent circuits

5.7.1 Gas sensing mechanism of PS semiconductor

A complete understanding of the details of this transduction process has not yet been established, and, as such, this report's intent is to provide an approximation to the electrical and chemical reactions that govern the operation of the PS semiconductor (Figs. 18, 19, 20).

5.7.2 Chemical reaction of PS semi by hydrogen bonds

Under DC conditions, the sensitivity of the sensor is poor and this dc analysis for gas sensing makes use of the larger surface to volume of the PS; the ac analysis is better due to reduced substrate leakage current by the skin effect, and hence, the AC Impedance metric is chosen for gas sensing applications. The mechanism of alcohol sensing involves the interaction between the hydrogen ions and the nanoporous surface of the sensor which forms the ethoxide ions on the surface of the PS. The electrons present in the PS move from the valence band into the conduction band forming a space charge on the surface of the PS. The ionic hydrogen species react with the ethoxide, thereby trapping the electrons and releasing them onto the surface of the PS and then into the gas. This reduces the mobility of the electrons present in the nanopores of the PS semiconductor that causes an increase in the resistance on the surface of the porous silicon. This surface charge reaction rate is greatly affected by boundary conditions, such as ac, dc, pressure, temperature, humidity, baseline drift etc.
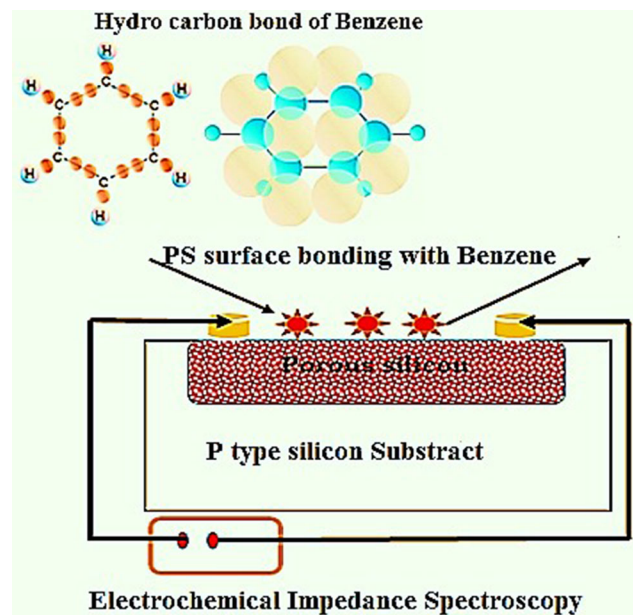

Fig. 20 Surface change in charge mobility of electron by benzene bond

6 Conclusion

The fabricated PS gas sensing device responded well at room temperature and at different concentrations of benzene, butane and methane gas. The porous silicon was composed of nanopores. The PS sensor was able to detect benzene, butane and methane gas at room temperature at concentrations ranging from 2 to 16 ppm. The sensor response and recovery is about 2 s and 6 s respectively. The selectivity and repeatability of the sensor response is the maximum when compared to other interfering gases.
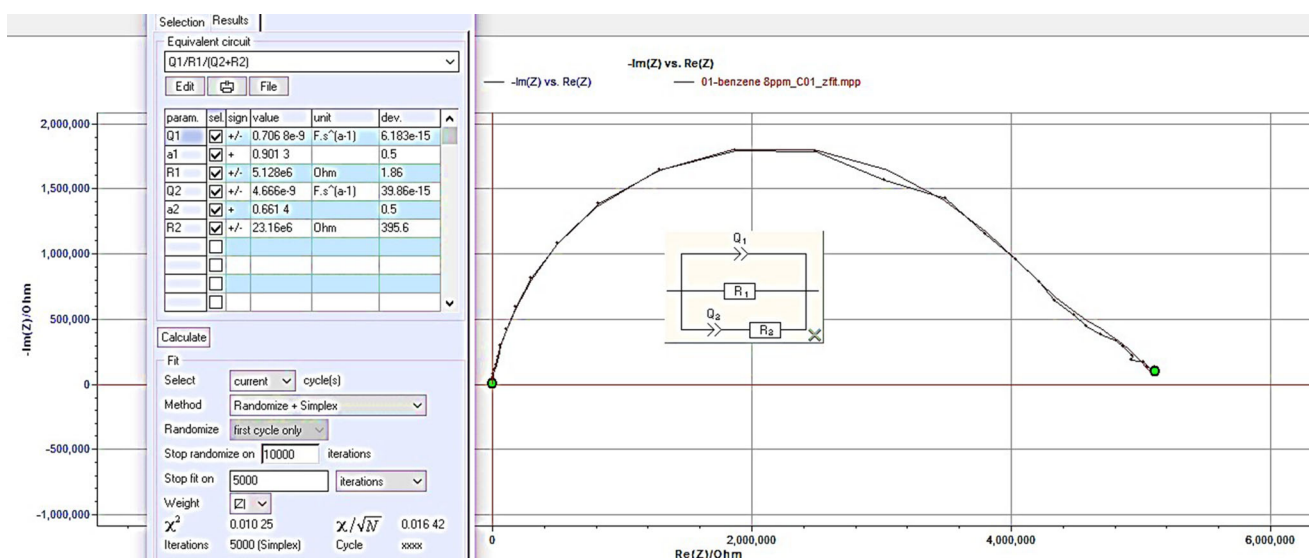

Fig. 19 Sensor repeatability of the PS based gas sensor

The grain boundary resistance values increased with an increase in the gas concentration, thus indicating the performance of a stable PS gas sensor even in a low ppm range at room temperature. The Fusion of the transduction mechanism in the Micro and Macro nanopores of the Porous silicon semiconductor (PS) was employed to fabricate an MEMS-based aliphatic alcohol impedance sensor. The presence of a nanopore network on silicon was confirmed by the SEM image. The morphology of the PS nanopores was roughly distributed in a uniform manner. The performance of the sensor was studied using Impedance spectroscopy at room temperature. Electrochemical impedance spectroscopy (EIS) and an equivalent circuit analysis of the small amplitude ($\pm$ 10 mV) AC impedance measurements (frequency range 0.1 Hz–1 kHz) at ambient temperature were carried out. The Sensing layer consists of nanopores (45.30–71.13 nm), micropores (0.95–5 µm), and comb type alumina electrodes with the micro PS layer having a thickness of about 0.2 µm and macro PS layer having a thickness of about 4 µm. These results were used to assess the effect of the micro PS and macro PS of the particulate layer on the conductivity of the given aliphatic gases. The calculated impedance was approximately 2.3e5 for the Micro PS, and 3.22e5 for the Macro PS for 8 ppm of gas injected into the gas chamber. The grain boundary resistance increases with an increase in the concentration of butane, benzene, and methane, which ranges from 2 to 16 ppm.

References

Badilla JP, Rojas DC, Lopez V, Fahlman BD, Ramirez-Porras A (2011) Development of organic vapour sensor based on functionalized porous silicon. Phys Status Solidi A 208(6):1458–1461

du Plessis M (2007) Properties of porous silicon nano-explosive devices. Sens Actuators A 135:666–674

Dusheiko M, Ilchenko V, Obukhova T, Stepanova M (2017) Sensors on FET with porous silicon. In: 37th International conference on electronics and nanotechnology (ELNANO). IEEE, Kiev, Ukraine. https://doi.org/10.1109/ELNANO.2017.7939739

Escorcia-Garcia J, Martinez OS, Gracia-Jimenez JM, Agarwal V (2009) Porous silicon photonic devices using pulsed anodic etching of lightly doped silicon. J Phys D Appl Phys 42:145101–145108

Gessner T et al (2000) Metal oxide gas sensor for high temperature application. Microsyst Technol 6:169–174

Kanungo J, Basu S (2014) Ohmic and rectifying contacts to porous silicon. In: Canham L (ed) Handbook of porous silicon. Springer, Cham. https://doi.org/10.1007/978-3-319-04508-5_72-1

Kanungo J, Pramanik C, Bandopadhyay S, Gangopadhyay U, Das L, Saha H, Gettens RT (2006) Improved contacts on a porous silicon layer by electroless nickel plating and copper thickening. Semicond Sci Technol 21:964

Kanungo J, Maji S, Saha H, Basu S (2009) Stable aluminium ohmic contact to surface modified porous silicon. Solid State Electron 53(6):663–668

Karacali T, Hasar UC, Ozbek IY, Oral EA, Efeoglu H (2013) Novel design of porous silicon based sensor for reliable and feasible chemical gas vapor detection. J Lightwave Technol 31(2):295–305

Losic D, Santos A (2015) Electrochemically engineered nanoporous materials. Springer Series in Materials Science. Springer, Berlin, p 220

Mabrook M, Ray A, Ghassemlooy Z, Brown S (1995) Electrical characteristics of metal contacts on porous silicon. In: IEE colloquium on materials for displays. London, UK. https://doi.org/10.1049/ic:19950981

Ogata YH, Koyama A, Harraz FA, Salem MS, Sakkaa T (2007) Electrochemical formation of porous silicon with medium-sized pores. Electrochemistry 75(3):270–272

Palzer S, Moretton E, Ramirez FH, Romano-Rodriguez A, Wöllenstein J (2008) Nano-and microsized metal oxide thin film gas sensors. Microsyst Technol 14:645–651

Pérez EX (2008) Design, fabrication and characterization of porous silicon multilayer optical devices. Universitat Rovira i Virgili, Chicago

Sailor MJ (2012) Fundamentals of porous silicon preparation. In: Porous silicon in practice: preparation, characterization and applications. Wiley-VCH Verlag GmbH & Co. KGaA, pp 1–42. https://doi.org/10.1002/9783527641901.ch1

Selvakumar VS, Sujatha L (2019) A parametrical study of porous silicon for volatile organic chemical sensor applications. Sens Lett 17(5):405–410

Selvakumar VS, Sujatha L, Suganthi S, Kumar SS (2019) Fabrication of nanoparticles based nanoporous silicon sensor for detection of volatile organic compounds. Sens Lett 17:423–430

Sujatha L, Bhattacharya E (2007a) Composite silicon/porous silicon membranes for low pressure sensors, IUMRSICAM

Sujatha L, Bhattacharya E (2007b) Sensitivity and stress in pressure sensors with composite silicon/macroporous silicon membranes. In: International workshop on physics of semiconductor devices. IEEE, Mumbai, India. https://doi.org/10.1109/IWPSD.2007.4472626

Valera E, Casals O, Vetter M, Rodriguez A (2007) Micro porous silicon gas sensor based on inter digitated micro electrodes, 1-4244-0869-5/07 IEEE. pp 197–200

Vinod PN (2005) Specific contact resistance of the porous silicon and silver metal Ohmic contact structure. Semicond Sci Technol 20(9):966

Wang YH, Lee CY, Lin CH, Fu LM (2008) Enhanced sensing characteristics in MEMS-based formaldehyde gas sensors. Microsyst Technol 14:995–1000

Zhang GX (2005) Porous silicon: morphology and formation mechanisms, modern aspects of electrochemistiy, vol 39. Springer, New York

Zhang D, Wang K, Tong J, Xia B (2014) Characterization of layer-by-layer nano self-assembled carbon nanotube/polymer film sensor for ethanol gas sensing properties. Microsyst Technol 20:379–385